
# Searching Discontinuous and Jump Points in Physical Discontinuities with Adaptive Phase Unwrapping

Yao-ting Zhang[1], Min-Jui Huang[2] and Tsung-Yeh Tsai[3]

[1]National Chung-Hsing University of Taiwan, ting@ctu.edu.tw
[2]National Chung-Hsing University of Taiwan, mjhuang@dragon.nchu.edu.tw
[3]National Chung-Hsing University of Taiwan, g9761115@mail.nchu.edu.tw

**ABSTRACT**

This study proposes a method of detecting discontinuous points in physical discontinuities in light intensity fringe pattern (IFP). After changing the experimental conditions, several images were captured with CCD and converted into wrapped phase maps with phase shifting technology (PST). In low-noise wrapped phase maps, discontinuous and jump points were searched directly; and in high-noise wrapped phase maps, these points were searched after filtering. Noise discontinuous points were screened by image comparison to correctly select physical discontinuous points. The location of physical discontinuities was marked according to the assembly principle to prevent diffusion on both sides along the discontinuous line by phase unwrapping from crossing the line. In doing so, the surface appearance of the specimen was phase unwrapped successfully.

**Keywords:** discontinuous point, phase shifting, phase unwrapping, block assembly.
**DOI:** 10.3722/cadaps.2012.385-395

## 1 INTRODUCTION

Optical interferometry provides non-contact, non-destructive and full-field surface topography inspection. The common interferometry methods include the Michelson interferometry[1], holography interferometry[2], electronic speckle pattern interferometry (ESPI)[3], satellite radar interferometry[4] and structured light[5]. With experiment implementation and image capturing, a light intensity fringe pattern (IFP) were captured with black and white is obtained with any of them. Physically, IFP represents the surface change of surface topography. By changing the experimental conditions with the phase shifting technology (PST)[6,7], phase shiff is produced in each light IFP. After solving the simultaneous equation, the wrapped phase map $\phi(x,y)$ is obtained.

Due to arctangent computing, the phase changes within the cycle between $-\pi/2$ and $+\pi/2$ in a phase shifting. Ghiglia[8] thus proposed the Cellular Automata phase unwrapping method to determine if it is necessary to compensate a $\pm 2\pi$ phase to raw wrapped maps of such kind. Spik[9] increased the original four adjacent points to eight points to not only shorten the computing time but also deal with low-noise discontinuity problems. Huang[10] proposed the adaptive parallel phase unwrapping method to successfully solve problems in small-angled shearing with high noise.

This study proposes a method for searching and blocking physical discontinuities in high-noise wrapped phase maps to prevent incorrect phase unwrapping of two discontinuous surfaces. In this

method, discontinuous and jump points were searched and filtered in order to locate the points of physical discontinuities. Then, the shear line was marked according to the assembly principle. Lastly, phase unwrapping was completed.

## 2 SEARCHING DISCONTINUOUS AND JUMP POINTS IN PHYSICAL DISCONTINUITIES

### 2.1 Phase Shifting Technology and Phase Unwrapping

With PST, the mathematical expression of the light IFP is shown in equation (1). In (1), B(x,y) represents background intensity, A(x,y) adaptive intensity, and $\phi$(x,y) the phase value. These three unknown equations need at least three light IFPs to find out the phase value. Therefore, the experimental condition needs to be changed to produce the phase shift $\delta_n$. Different measuring technologies need different PSTs. Assume that the adjustable phase value in each phase shift is π/2, $\delta_1$=0, $\delta_2$=π/2, $\delta_3$=π and $\delta_4$=3π/2. Equation (2), wrapped phase map where $\phi$(x,y), was obtained after solving the equation:

$$I_n(x,y) = B(x,y) + A(x,y)\cos\left(\phi(x,y) + \delta_n\right) \tag{1}$$

$$\Rightarrow \phi(x,y) = Tan^{-1}\left(\frac{I_4(x,y) - I_2(x,y)}{I_1(x,y) - I_3(x,y)}\right) \tag{2}$$

The change of the arctangent value falling within the cycle between -π/2 and +π/2 is known as π-modulus. Based on the positive or negative sign of the numerator, sin$\phi$, and the denominator, cos$\phi$, the value of the phase value in the quadrant falling between –π and +π is determined. It is also known as 2π-modulus. The determination of the phase value in the quadrant is shown in Figure 1.

| cos \ sin | + | - |
|---|---|---|
| + | $\phi$ | $\phi$ |
| - | $\phi + \pi$ | $\phi$ - $\pi$ |

Fig. 1: Determination of phase value in the quadrant.

According to the path-independent phase unwrapping technology (PUT), the unwrapping of a point (±2π) is determined with reference to the phase difference between the unwrapping and adjacent points. Assuming that the phase value before and after unwrapping is $\phi$(x,y) and $\phi$'(x,y) respectively, the mathematical logic is expressed as follows:

$$\phi'_{(x,y)} = \phi_{(x,y)} + 2\pi \cdot \text{int}\left(\frac{\phi_{(x,y)} - \phi_0}{2\pi}\right) \tag{3}$$

$$\phi_0 = \phi_{(x-1,y)}$$

In this expression, $\phi_0$ represents the phase value of the reference adjacent point and $\text{int}(\phi)$ the closest integer function.

## 2.2 Search of Discontinuous Points and Jump Points

According to Goldstein [11], a closed path (Figure 2) is formed by linking discontinuous points with the four-point surround method on a phase map using the 2x2 mask after calculating the summation of phase difference with the following mathematical computing logic:

$$S(i,j)=\text{int}\left[\frac{\phi(i+1,j)-\phi(i,j)}{2\pi}\right]+\text{int}\left[\frac{\phi(i+1,j+1)-\phi(i+1,j)}{2\pi}\right]+\text{int}\left[\frac{\phi(i,j+1)-\phi(i+1,j+1)}{2\pi}\right]+\text{int}\left[\frac{\phi(i,j)-\phi(i,j+1)}{2\pi}\right] \quad (4)$$

where int represents the nearest integer function; when S(i,j)=0, it is a continuous point, when S(i,j)=+1, it is a positive discontinuous point, when S(i,j)=-1, it is a negative discontinuous point, indicating on the upper left corner $\phi$(i,j). As shown in Figure 3, Although the discontinuous points along the shear line in a low-noise wrapped map are determined with Goldstein's method(as shown in Figure 3(b)), erroneous determination occurs as shown in Figure 3(d) when there are phase differences due to high noise.

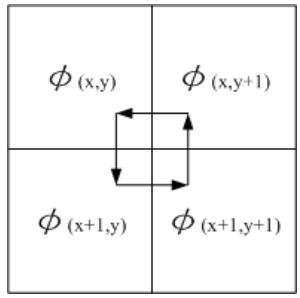


Fig. 2: Illustration of four-point surround test.

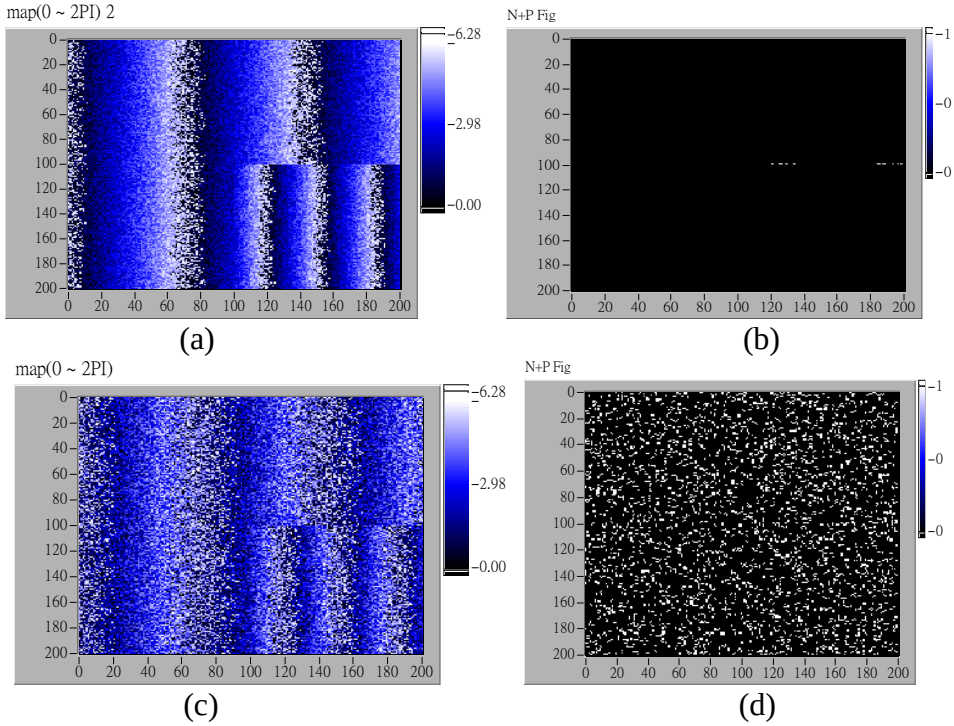


Fig. 3: Search of discontinuous points with the four-point surround method: (a) Low-noise wrapped phase map with shear lines; (b) Locations with intractable discontinuous points; (c) High-noise (2 times low noise) wrapped phase map with shear lines; (d) Unidentified discontinuous points formed by discontinuous points and noise.

wrapped phase maps with higher noise must be filtered first. Generally, mean filtering adjusts the data on the jump line to their mean, and this will result in data loss of jump points. By applying sine-cosine mean filtering to individual jump points and reducing the value region into the arctangent, the noise is removed without phase distortion (Figure 1(b)). The mathematical computing logic is as follows:

$$\overline{\psi}_{m,n} = Tan^{-1} \frac{\frac{\sum \sin \psi_{i,j}}{k^2}}{\frac{\sum \cos \psi_{i,j}}{k^2}} \tag{5}$$

where $k$ is the mask size for filtering: $i = m + g$ and $j = n + h$

$$\begin{cases} g = \dfrac{(1-k)}{2} \sim \dfrac{(k-1)}{2} \\ h = \dfrac{(1-k)}{2} \sim \dfrac{(k-1)}{2} \end{cases} \tag{6}$$

As shown in Figure 4, when searching discontinuous points after sine-cosine mean filtering, although some discontinuous points are reduced in the shearing process, discontinuous points formed by noise will all be filtered.

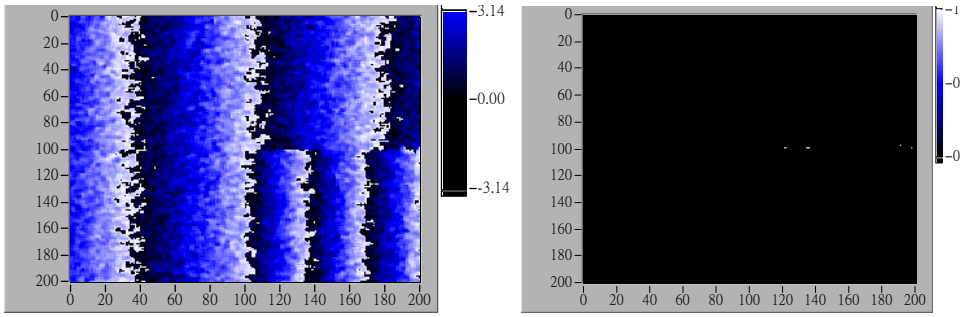


Fig. 4: Search of discontinuous points after sine-cosine mean filtering: (a) Results of sine-cosine mean filtering of Figure 3(c); (b) Results of the search of discontinuous points.

Several discontinuous points on the shear line are located with the above methods. As there are inadequate reference points on the shear line, we must capture the seams between the physical discontinuous points with jump points. As the phase jump is another type of discontinuity that is formed by arctangent calculation of the wrapped phase map, it can display the discontinuity of shear lines. When the absolute value of the phase difference between a point and its adjacent point on a wrapped phase distribution map is greater than π, this pixel is known as a jump point, and its mathematical logic is expressed as follows:

$$\begin{cases} R(i,j) = 1, & \left|\phi(i+m, j+n) - \phi(i,j)\right| \geq \pi, \quad m,n = -1,0,+1 \\ R(i,j) = 0, & \left|\phi(i+m, j+n) - \phi(i,j)\right| < \pi, \quad m,n = -1,0,+1 \end{cases} \tag{7}$$

When R(i,j)=0 is defined as a non-jump point and R(i,j)=1 a jump point, this suggests that the wrapping effect may take place at this pixel point (i,j), and a shift at 2π times must be assigned. The line segment formed with the jump points is called a jump line. A correct jump line must form a closed loop with either the phase map boundary or itself in order to cut the phase distribution map into several blocks. In terms of block PUT, all pixels in the same block are homogeneous.

Figure 5(a) shows the direct search of jump points in a high-noise wrapped phase map with shear lines. Figure 5(b) shows the search of jump points in a high-noise wrapped phase map after sine-cosine mean filtering. It is clear only after sine-cosine mean filtering that there are adequate reference jump

points to form a jump line. The jump line here is formed by the wrapped phase jump points, noise jump points and shear line jump points.

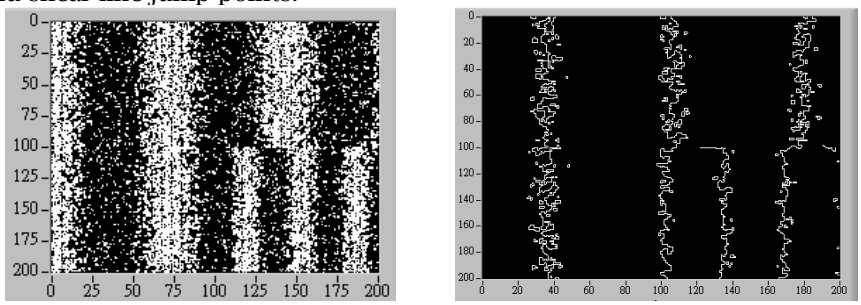


(a) (b)

Fig. 5: Results of jump point search: (a) Direct search of jump points in a high-noise wrapped phase map with shear lines; (b) Search of jump points in a high-noise wrapped phase map after sine-cosine mean filtering.

In order to keep the shear line jump points by filtering the jump points in the wrapped phase map and noise jump points, we can modify the jump point parameter in (7), i.e. to modify the absolute value π of the phase difference with the adjacent points into a threshold value kπ as shown below:

$$\begin{cases} R(i,j)=1, & |\phi(i+m,j+n)-\phi(i,j)| \geq k_n\pi, \quad m,n=-1,0,+1 \\ R(i,j)=0, & |\phi(i+m,j+n)-\phi(i,j)| < k_n\pi, \quad m,n=-1,0,+1 \end{cases} \tag{8}$$

where $k_n$=0-2 and $k_1 < k_2$. In line segment display, the only adjacent points with a phase difference between $k_1\pi$ and $k_2\pi$ will be displayed. In this case, wrapped phase jump points with a phase difference at 2π with their adjacent points will be filtered by $k_2$-value; and noise jump points with a phase difference at near 0 with their adjacent points will be filtered by $k_1$ value. This is because the phase difference of both sides along the shear line is not a fixed value. Therefore, the threshold value $k_n$ must be adjusted for different phase maps in order to keep only the jump points on the shear line. Figure 6 shows that all noise jump points and wrapped phase jump points are filtered by adjusting the threshold value to $k_1$=0.4 and $k_2$=1.5 respectively, and only the shear line jump points remain.

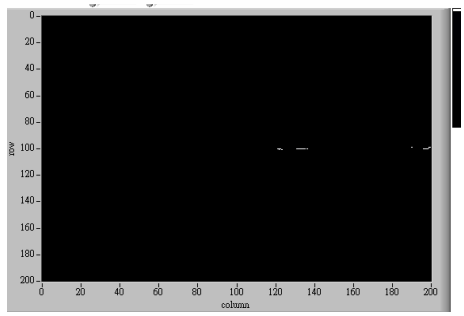


Fig. 6: Jump points of shear line by adjusting the threshold value to k=0.4-1.5.

### 2.3 The Assembly Line of Physical Discontinuities

Locating the jump points on the shear line by means of discontinuous point and jump point search, setting the point closet to the image boundary as the start point with the assembly line logic, forming a line with other nearest start points etc., the line assembly sequence is obtained. As shown in Figure 7, Point A is the closet to the boundary and thus set as the start point of the line. A line is form by linking in order points A to D according to the following sequence: A→B→C→D. Any two points are linked with a straight line. If there is adequate data, a straight line formed with several segments will highly match with the original shear line. Lastly, it is time to determine if it is necessary to link Point A to the boundary. If the shear line is located in the image, i.e. without penetrating the image, the

discontinuous points of the start and end points are with the opposite sign, and there is no need to link to the boundary. All points on line AB with the same sign are linked and extended to the boundary.

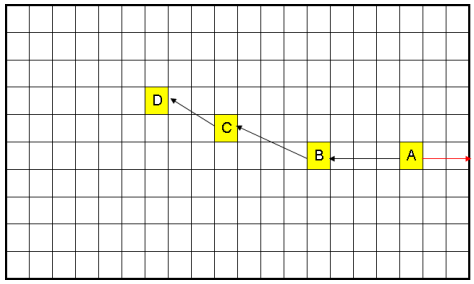


Fig. 7: Illustration of point assembly logic.

Discontinuous points with the same sign suggest that the gradient change of both sides of a shear line is identical, and the shear is in progress. If the sign is opposite, this suggests a change of the gradient, and the shear is diminishing. This mathematical logic also allows us to determine if the shear line links to the boundary. Figure 8 shows the testing results where the shear line in a discontinuous form is correctly marked. Figure 9 shows the results of a test using curve shear in a noise wrapped phase map. The curve shear line is also marked correctly. In this example, the image shear line runs across (penetrates) the entire image.

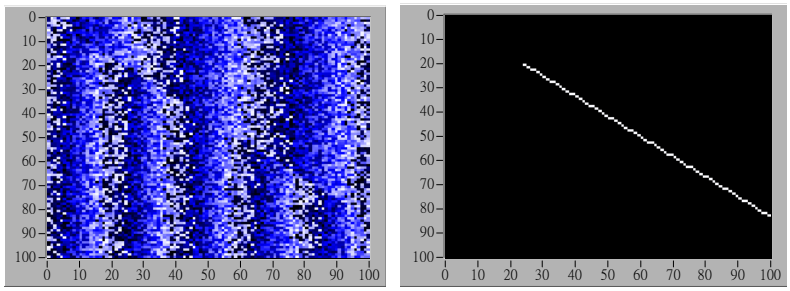


(a) (b)

Fig. 8: Noise wrapped phase map assembly with an oblique shear line: (a) Wrapped phase map with a straight shear line; (b) Results of assembly with searched discontinuous and jump points.

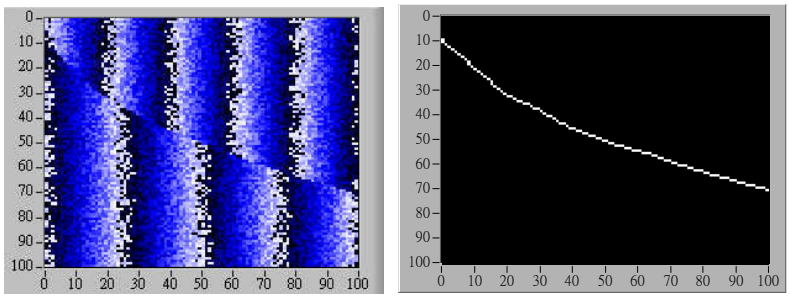


(a) (b)

Fig. 9: Noise wrapped phase map assembly with a curve shear line: (a) Wrapped phase map with a curve shear line; (b) Results of assembly with searched discontinuous and jump points.

### 2.4 Marking and Blocking of Physical Discontinuities

The phase value of both sides of a shear line is independent and relationship. In the case as shown in Figure 8, as phase unwrapping bypasses the shear line, the entire image remains intact. By contrast, the image is bisected in the case as shown in Figure 9 where phase unwraps independently on each

side. Next, it is to mark the discontinuous points of physical discontinuity and set the shear line as the boundary where phase unwrapping stops. Therefore, by searching the discontinuous and jump points after sine-cosine mean filtering in the example as shown in Figure 8, the assembly line and markings are blocked. Lastly, the results of phase unwrapping are shown in Figure 10. In Figure 9, the two physically discontinuous regions can be unwrapped as two independent wrapped phase maps as there is no phase relationship between them. As the correct phase is obtainable after comparing the adjacent images, including upper, lower, left and right, we can only unwrap the phase as shown in Figure 11.

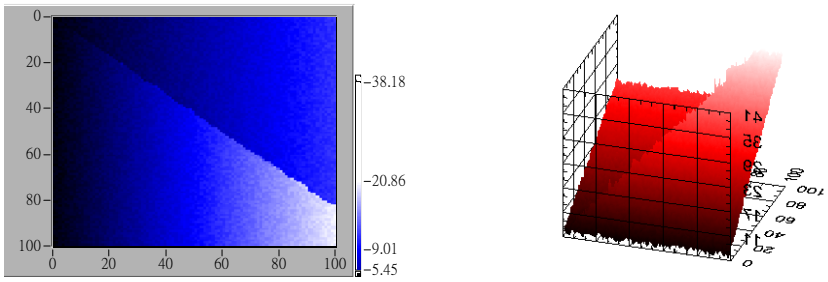


(a) (b)

Fig. 10: Unwrapping of a high-noise phase wrapped map with straight shear lines: (a) Real phase map after high-noise unwrapping with a straight shear line; (b) 3D output results of the same phase map.

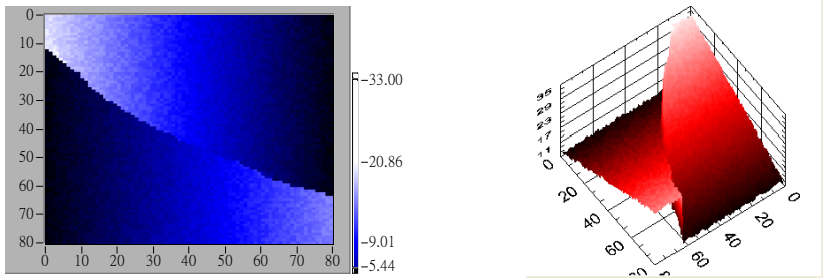


(a) (b)

Fig. 11: Unwrapping of a high-noise phase wrapped map with curve shear lines: (a) Real phase map after high-noise unwrapping with a curve shear line; (b) 3D output results of the same phase map.

## 3 THE PRINCIPLE OF BLOCK ASSEMBLY

### 3.1 Advantages of Block Assembly

According to the block assembly theory (BAT) [12], a map is split into several blocks for individual phase unwrapping. After the phase wrapping of each block is completed, the phase of individual blocks is compared with that of their adjacent blocks. By eliminating the phase difference between sub-blocks, we can completely phase unwrapping of the original phase map. The manner of split is free, depending on the size of images. The advantages of map split include: (1) optimal unwrapping parameters for individual sub-blocks to save computing time as the characteristics of phases in individual blocks vary; (2) errors in one block will not affect the entire map because phase unwrapping is block-independent, and errors in moving or physical discontinuity will be restricted in only the respective block, making it easier to eliminate such errors.

BAT becomes more important to digital still cameras with higher resolutions (i.e. more pixels). In addition to reducing phase computing time, each small block can be considered as a large dot in DSCs with over one mega pixels. When physical discontinuity diffuses in any block, we can almost discard this block without affecting the resolution of the entire image, as long as block assembly after phase unwrapping succeeds. Therefore, for images with high resolutions, isolating problematic blocks and correctly assembling these blocks will be more important than searching discontinuous points.

### 3.2 Mathematical Logic of Block Assembly

Figure 12 shows an image split into nine even blocks; i.e. 3 by 3. When comparing the block boundary of the left and right adjacent blocks, A and B, there is a big difference in the value between the two adjacent points as a result of noise and phase jump. However, the phase value of the two adjacent boundary points should be close to each other due to image continuity. The mean phase difference of the two boundary points of these two blocks is $\Delta\phi_{AB}$, this represents the phase difference of all points within the same block. Therefore, by calculating the cumulative mean phase difference of all points of a phase map with a lower mean difference, the true phase map is obtained. The upper and lower adjacent blocks, A and C, can also be assembled in the same way according to the following mathematical logic:

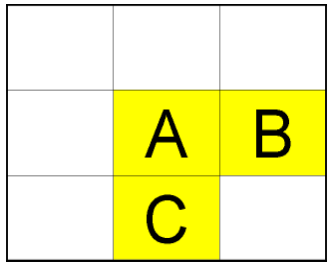


Fig. 12: An image split in 9 even blocks (3 by 3).

$$A_{m,n}=\begin{bmatrix} a_{11} & a_{12} & a_{13} & a_{14} & \cdot & \cdot & \cdot & \cdot & a_{1n} \\ a_{21} & a_{22} & a_{23} & a_{24} & \cdot & \cdot & \cdot & \cdot & a_{2n} \\ a_{31} & a_{32} & a_{33} & a_{34} & \cdot & \cdot & \cdot & \cdot & a_{3n} \\ a_{41} & a_{42} & a_{43} & a_{44} & \cdot & \cdot & \cdot & \cdot & a_{4n} \\ \cdot & & & & & & & & \cdot \\ \cdot & & & & & & & & \cdot \\ \cdot & & & & & & & & \cdot \\ \cdot & & & & & & & & \cdot \\ a_{m1} & a_{m2} & a_{m3} & a_{m4} & \cdot & \cdot & \cdot & \cdot & a_{mn} \end{bmatrix} B_{m,n}=\begin{bmatrix} b_{11} & b_{12} & b_{13} & b_{14} & \cdot & \cdot & \cdot & \cdot & b_{1n} \\ b_{21} & b_{22} & b_{23} & b_{24} & \cdot & \cdot & \cdot & \cdot & b_{2n} \\ b_{31} & b_{32} & b_{33} & b_{34} & \cdot & \cdot & \cdot & \cdot & b_{3n} \\ b_{41} & b_{42} & b_{43} & b_{44} & \cdot & \cdot & \cdot & \cdot & b_{4n} \\ \cdot & & & & & & & & \cdot \\ \cdot & & & & & & & & \cdot \\ \cdot & & & & & & & & \cdot \\ \cdot & & & & & & & & \cdot \\ b_{m1} & b_{m2} & b_{m3} & b_{m4} & \cdot & \cdot & \cdot & \cdot & b_{mn} \end{bmatrix} \tag{9}$$

$$C_{m,n}=\begin{bmatrix} c_{11} & c_{12} & c_{13} & c_{14} & \cdot & \cdot & \cdot & \cdot & c_{1n} \\ c_{21} & c_{22} & c_{23} & b_{24} & \cdot & \cdot & \cdot & \cdot & c_{2n} \\ c_{31} & c_{32} & c_{33} & c_{34} & \cdot & \cdot & \cdot & \cdot & c_{3n} \\ c_{41} & c_{42} & c_{43} & c_{44} & \cdot & \cdot & \cdot & \cdot & c_{4n} \\ \cdot & & & & & & & & \cdot \\ \cdot & & & & & & & & \cdot \\ \cdot & & & & & & & & \cdot \\ \cdot & & & & & & & & \cdot \\ c_{m1} & c_{m2} & c_{m3} & c_{m4} & \cdot & \cdot & \cdot & \cdot & c_{mn} \end{bmatrix}$$

The real phase value of Blocks B and C after assembly is $B'_{m,n}$ and $C'_{m,n}$ respectively.

$$\Delta\phi_{AB}=\frac{1}{m}\sum_{i=1}^{m}\left[a_{in}-b_{i1}\right] \tag{10}$$

$$B'_{m,n}=\begin{bmatrix} b_{11}+\Delta\phi_{AB} & b_{12}+\Delta\phi_{AB} & b_{13}+\Delta\phi_{AB} & b_{14}+\Delta\phi_{AB} & \cdot & \cdot & \cdot & \cdot & b_{1n}++\Delta\phi_{AB} \\ b_{21}+\Delta\phi_{AB} & b_{22}+\Delta\phi_{AB} & b_{23}+\Delta\phi_{AB} & b_{24}+\Delta\phi_{AB} & \cdot & \cdot & \cdot & \cdot & b_{2n}+\Delta\phi_{AB} \\ b_{31}+\Delta\phi_{AB} & b_{32}+\Delta\phi_{AB} & b_{33}+\Delta\phi_{AB} & b_{34}+\Delta\phi_{AB} & \cdot & \cdot & \cdot & \cdot & b_{3n}+\Delta\phi_{AB} \\ b_{41}+\Delta\phi_{AB} & b_{42}+\Delta\phi_{AB} & b_{43}+\Delta\phi_{AB} & b_{44}+\Delta\phi_{AB} & \cdot & \cdot & \cdot & \cdot & b_{4n}+\Delta\phi_{AB} \\ \cdot & & & & & & & & \cdot \\ \cdot & & & & & & & & \cdot \\ \cdot & & & & & & & & \cdot \\ \cdot & & & & & & & & \cdot \\ b_{m1}+\Delta\phi_{AB} & b_{m2}+\Delta\phi_{AB} & b_{m3}+\Delta\phi_{AB} & b_{m4}+\Delta\phi_{AB} & \cdot & \cdot & \cdot & \cdot & b_{mn}+\Delta\phi_{AB} \end{bmatrix} \tag{11}$$

$$\Delta\phi_{AC} = \frac{1}{n}\sum_{j=1}^{n}\left[a_{mj} - c_{1j}\right] \tag{12}$$

$$C'_{m,n} = \begin{bmatrix} c_{11}+\Delta\phi_{AC} & c_{12}+\Delta\phi_{AC} & c_{13}+\Delta\phi_{AC} & c_{14}+\Delta\phi_{AC} & \cdots & c_{1n}+\Delta\phi_{AC} \\ c_{21}+\Delta\phi_{AC} & c_{22}+\Delta\phi_{AC} & c_{23}+\Delta\phi_{AC} & b_{24}+\Delta\phi_{AC} & \cdots & c_{2n}+\Delta\phi_{AC} \\ c_{31}+\Delta\phi_{AC} & c_{32}+\Delta\phi_{AC} & c_{33}+\Delta\phi_{AC} & c_{34}+\Delta\phi_{AC} & \cdots & c_{3n}+\Delta\phi_{AC} \\ c_{41}+\Delta\phi_{AC} & c_{42}+\Delta\phi_{AC} & c_{43}+\Delta\phi_{AC} & c_{44}+\Delta\phi_{AC} & \cdots & c_{4n}+\Delta\phi_{AC} \\ \vdots & & & & & \vdots \\ c_{m1}+\Delta\phi_{AC} & c_{m2}+\Delta\phi_{AC} & c_{m3}+\Delta\phi_{AC} & c_{m4}+\Delta\phi_{AC} & \cdots & c_{mn}+\Delta\phi_{AC} \end{bmatrix} \tag{13}$$

## 4 EXPERIMENT

As shown in Figure 13, In the ESPI experiment, the hardware included (1) PC—Intel Pentium Dual Core E6500 2.93GHz, (2) RAM—1.96GB, (3) video capture card—PCI-1408, (4) data capture card—PCI-MIO-16XE-10, (5) black and white digital camera—PULNIX-TM-7CN, and (6) Piezoelectric ceramic(PZT) —P840.60, and the software is Labview7.1.

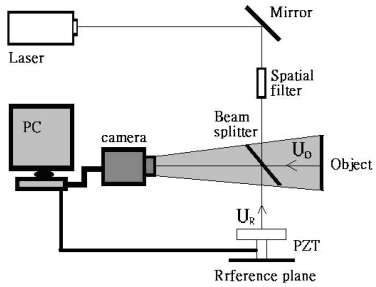


Fig. 13: ESPI experiment implementation.

The PC drives the data capture card (PCI-MIO-16XE-10) to activate the PZT (P840.60) to generate four phase shifts: $\delta_1$=0, $\delta_2$=π/2, $\delta_3$=π and $\delta_4$=3π/2. Eight light IFPs before and after deformation as shown in Figure 14 were captured with the CCD (PULNIX-TM-7CN) and video capture card (PCI-1408). Four light IFPs were converted into the wrapped phase map as shown in Figure 15 with PST. Discontinuous line segments as shown in Figure 16 were obtained with the search of discontinuous and jump points and line assembly theory. The phase as shown in Figure 17 was obtained after phase unwrapping with BAT.

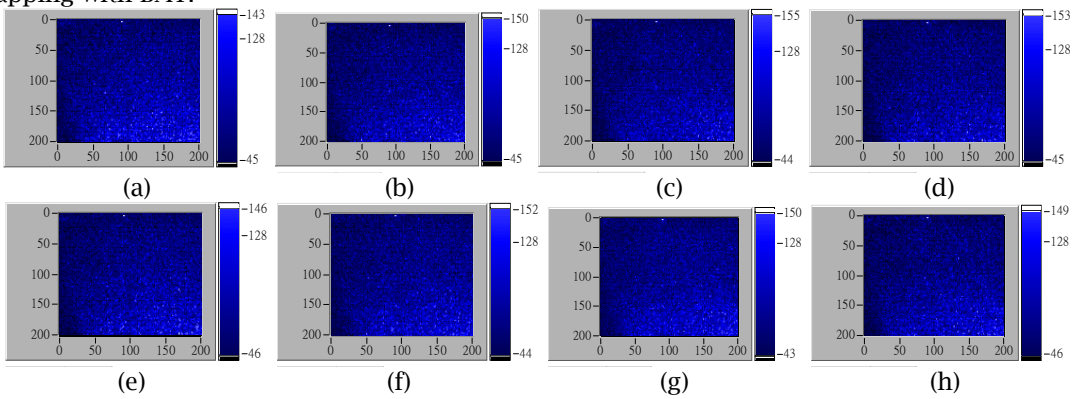


Fig. 14: Light IFPs before deformation (a) $\delta_1$=0 (b) $\delta_2$=π/2 (c) $\delta_3$=π (d) $\delta_4$=3π/2, Light IFPs after deformation (e) $\delta_1$=0 (f) $\delta_2$=π/2 (g) $\delta_3$=π (h) $\delta_4$=3π/2.

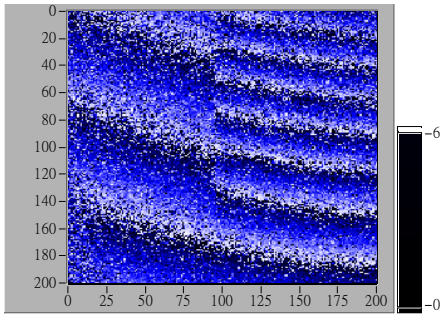


Fig. 15: Wrapped phase map after phase shifting.

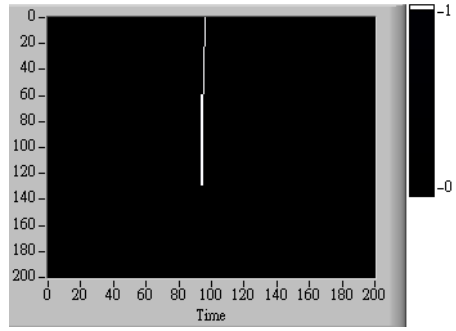


Fig. 16: Physical discontinuous lines.

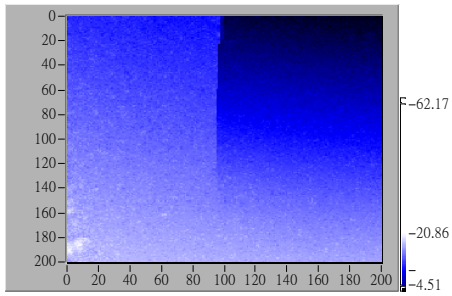


(a)

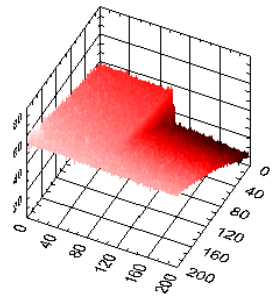


(b)

Fig. 17: Phase map after phased unwrapping: (a) Real phase map after high-noise unwrapping with a shear line; (b) 3D output results of the same phase map.

Figure 18 shows the results of phase unwrapping in blocks split from the high-noise wrapped phase map with physical discontinuities as shown in Figure 15. Comparing the phase unwrapping (computing) time of individual blocks, it takes about 674.966 seconds to unwrap a 200x200 map without splitting. After splitting it into four even blocks (4x4), the unwrapping time is reduced to 39.156 seconds. Also, results show that the phase unwrapping time difference of a map split less than 50x50 blocks is small. This suggests that block split is very important to the phase unwrapping of DSCs with higher resolutions.

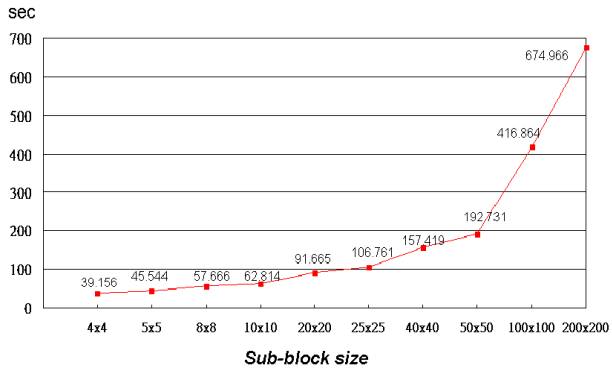


Fig. 18: Phase unwrapping time of blocks in different sizes.

## 5 CONCLUSIONS

High noise and physical discontinuity are the main causes of errors in phase unwrapping. Although adaptive parallel phase unwrapping is a great solution for unwrapping high-noise wrapped phase maps, when high noise and physical discontinuity are found in the same map, a method to search,

identify and block unwrapping errors is needed. The aim of this study is to propose an integrated solution for searching discontinuous and jump points in order to locate the physically discontinuous points and filter the influence of high noise, and assemble, mark and block the erroneous paths of phase unwrapping. When unwrapping high-resolution images (with more pixels), the image can be split into many blocks. By unwrapping the phase map of individual blocks and by capturing the boundary phase difference of blocks by means of BAT, we can shorten the unwrapping (computing) time of the entire image.

Noise and physical DUT discontinuities are unavoidable in any optical inspection due to differences in experimental methods and conditions. Although noise filtering and phase unwrapping technologies are rather mature, no ideal and appropriate method for identifying physical discontinuities has been realized. Therefore, to develop a method that can directly mark all physical discontinuities will be the target of future study.

## REFERENCES


[1] Mayorga-Cruz, D.; M'arquez-Aguilar, P. A.; Sarmiento-Martinez, O.; Uruchurtu-Chavarin, J.: Evaluation of corrosion in electrochemical systemsusing Michelson interferometry, Optics and Lasers in Engineering, 45, 2007, 140-144. doi:10.1016/j.optlaseng.2006.02.001

[2] Cai M.; Liu D.: Study of failure mechanisms of rock under compressive– shear loading using real-time laser holography, International Journal of Rock Mechanics & Mining Sciences 46, 2009, 59-68. doi:10.1016/j.ijrmms.2008.03.010

[3] Dhanasekar B.; Ramamoorthy B.: Digital speckle interferometry for assessment of surface roughness, Optics and Lasers in Engineering 46, 2008, 272-280. doi:10.1016/j.optlaseng.2007.09.003

[4] Granam L. C.: Synthetic interferometry radar for topographic mapping, Proc. IEEE, vol.62, 1974, 763-768.

[5] Yu C.; Peng Q.: A correlation-based phase unwrapping method for Fourier-transform profilometry, Optics and Lasers in Engineering 45, 2007, 730-736. doi:10.1016/j.optlaseng.2006.10.006

[6] Bruning J. H.; Herriott D. R.; Gallagher J. E.; Rosenfeld D. P.; White A. D.; Brangaccio D. J.: Digital Wavefront Measuring Interferometer for Testing Optical surfaces and Lenses, Applied Optics, Vol.13, 1974, 2693-2703.

[7] Cheng Y. Y.; Wyant J. C.: Phase Shifter calibration in phase-shifting interferometry, Applied Optics, Vol.24, 1985, 3049-3052.

[8] Ghiglia D. C.; Mastin G. A.; Romero L. A.: Cellular-automata method for phase unwrapping, Optical Society America, Vol.4, 1987, 267-280.

[9] Spik A.; Robinson D. W.: Investigation of the cellular automata method for phase unwrapping and its implementation on an array processor, Optics and Lasers in Engineering 14, 1991, 25-37. doi:10.1016/0143-8166(91)90036-S

[10] Huang M. J.; Lai C. J.: Phase unwrapping based on a parallel noise-immune algorithm, Optics and Laser Technology, 2002, 457-464.

[11] Goldstein R. M.; Zebker H. A.; Werner C. L.: Satellite radar interferometry : Two-dimensional phase unwrapping, Radio Science, Vol.23, 1988, 713-720.

[12] Herraez M. A.; Burton D. R.; Lalor M. J.; Gdeisat M. A.: Fast two-dimensional phase-unwrapping algorithm based on sorting by reliability following a noncontinuous path, Applied Optics, Vol.41, 2002, 7437-7444.